Journal of Power Sources 195 (2010) 7540–7547

Contents lists available at ScienceDirect

Journal of Power Sources

journal homepage: www.elsevier.com/locate/jpowsour

Chromium transport by solid state diffusion on solid oxide fuel cell cathode

Grace Y. Lau[a,*], Michael C. Tucker[a], Craig P. Jacobson[a], Steven J. Visco[a], Stacy H. Gleixner[b], Lutgard C. DeJonghe[a]

[a] Materials Sciences Division, Lawrence Berkeley National Laboratory, 1 Cyclotron Rd., MS 62-203, Berkeley, CA 94720, USA
[b] Department of Chemical & Materials Engineering, San Jose State University, One Washington Square, Engineering 385, San Jose, CA 95192, USA

ARTICLE INFO

Article history:
Received 19 May 2010
Received in revised form 2 June 2010
Accepted 3 June 2010
Available online 15 June 2010

Keywords:
Solid oxide fuel cell
Stainless steel
Chromium
LSM
LSCF
LNF

ABSTRACT

Iron–chromium ferritic stainless steel is widely used in solid oxide fuel cell (SOFC) components. At 650–800 °C, stainless steels form a protective chromia oxide scale. This low conductivity catalytic compound can degrade SOFC cathode performance. The migration of Cr species onto the cathode occurs through vapor transport and/or solid state diffusion, and electrochemical reactions may affect the migration.

It is important to understand the relative Cr transport and reaction rates to evaluate the most viable commercially available cathode material. This study characterizes the migration of Cr species through solid state diffusion and vapor deposition. Chromia blocks and chromia-forming stainless steel interconnects were held in contact with LSM (Lanthanum Strontium Manganese Oxide), LSCF (Lanthanum Strontium Cobalt Ferrite) and LNF (Lanthanum Nickel Ferrite) perovskite pellets in Cr-saturated air at 700 °C for 300 h. XRD (X-ray Diffraction), SEM (Scanning Electron Microscope), EDS (Energy Dispersive X-ray Spectroscopy) and Ion Milling by FIB (Focused Ion Beam) were used to detect Cr on and within the perovskite pellets. Cr transport and reaction on LSCF is the most severe, followed by LSM. Cr transport is observed on LNF, but without noticeable reaction.

Published by Elsevier B.V.

1. Introduction

Over the past several decades, advancements have been made in the materials and cell fabrication technology to reduce the cost of the solid oxide fuel cells. One efficient way of reducing the raw material and fabrication cost is to lower the operating temperature of the SOFC (from 1000 to 600–800 °C) thereby enabling the use of stainless steel interconnects. Stainless steel, which consists primarily of iron and chromium, is inexpensive, robust and a good electrical conductor. Therefore, a lot of effort has been directed to lowering the operating temperature of the SOFC to a temperature range wherein oxidation of stainless steel interconnects is acceptable [1]. Stainless steel interconnects in the SOFC stack connect each cell in series, conduct electricity and separate the fuel and air atmospheres between the cells.

Although stainless steel interconnects can reduce the stack cost, they also introduce several challenges that hinder commercialization of the technology. At 650–800 °C, stainless steels form a scale, to minimize environmental attacks at the SOFC operating temperature [2]. Chromium oxide-forming alloys are always preferred due to their low electrical resistance, thus minimizing the ohmic loss within the stacks [1]. Chromium oxide scale can react with the cathode electrode, forming various non-catalytic compounds. These non-catalytic compounds increase the resistance of the fuel cell structure degrading the SOFC performance [1].

1.1. Effects of chromium transport

Lanthanum strontium manganese oxide $(La,Sr)MnO_3$ (LSM), lanthanum strontium cobalt ferrite $(La,Sr)(Co,Fe)O_3$ (LSCF) and lanthanum nickel ferrite $La(Ni,Fe)O_3$ (LNF) are the three chosen cathode material in this work. LSM, LSCF and LNF are known for their good electronic conductivity (130–580 S cm^{-1} at 800 °C) [2,3], compatibility with other components in the SOFC (LSM, LSCF and LNF have CTE-thermal expansion coefficient between 10 and 15×10^{-6} K^{-1} [2,3] which matches well with the CTE of the ceramic which have a range of 10.5×10^{-6}–12.5×10^{-6} K^{-1} [2,3]), and high catalytic activities at elevated temperatures [2–5].

Taniguchi et al. recorded the degradation of cell performance when alloy coupons were placed on the LSM cathode of the SOFC during cell tests [4]. The cell voltage decreased after 500 h of operation [4]. The decline of performance from ~700 to ~100 mV was attributed to the filling of pores by compounds of chromium oxide, which reduced the number of active electrode reaction sites [4]. This phenomenon was only observed when current was present;

* Corresponding author. Tel.: +1 510 486 5850; fax: +1 510 486 4881.
E-mail address: gylau@lbl.gov (G.Y. Lau).

0378-7753/$ – see front matter. Published by Elsevier B.V.
doi:10.1016/j.jpowsour.2010.06.017

no degradation of performance was observed when the cell was held at open circuit at 1000 °C for 300 h [4].

Taniguchi et al. also performed tests where various untreated stainless steel coupons were placed in contact with tablets of lanthanum chromite $LaCrO_3$ [4]. Degradation of cell performance was not observed for $LaCrO_3$. However, commercialization is unlikely because of the high cost of synthesizing $LaCrO_3$ [3].

Vaporization of hexavalent Cr from chromia-forming alloy surfaces was observed by Hilpert et al. [5]. Hexavalent Cr was reduced to Cr_2O_3 at the triple phase boundary (TPB) accompanied by reaction with LSM. The proposed degradation mechanisms according to Hilpert et al. are as follows [5]:

$$2CrO_2(OH)_2(g) + 6e^- \rightarrow Cr_2O_3(s) + 2H_2O(g) + 3O_2(g) \quad (1)$$

$$La_{1-x}Sr_xMnO_3(s) + (1/2)Cr_2O_3(s) \rightarrow La_{1-x}Sr_xMn_{1-y}Cr_yO_3(s) + (Cr_{1-y}Mn_y)O_{1.5-\delta}(s) + (\delta/2)O_2(g) \quad (2)$$

The deposition of the reaction products from Eq. (2) was predicted to inhibit the cathodic oxygen reduction reaction at the TPB. This could result in an increase in the electrode overpotential and hence, a decrease in the power output of the fuel cell [5].

Various effects of ferritic stainless steel on the performance of cathode-supported cells were observed by Jiang et al. [6–8]. Chromium deposits were observed on the electrolyte surface on both the reference electrode and the cathode in the presence of a cell overpotential, suggesting that deposition was caused not only by the reduction at the cathode/electrolyte interface, but also by the air flow [7]. This author suggested another mechanism which required Mn^{2+} to react with Cr to form Mn–Cr–O nuclei and act as nucleation sites for the crystallization and growth of Cr_2O_3 and $(Cr,Mn)_3O_4$ spinels [7]. Therefore, they concluded that under current, Mn^{2+} cations from the cathode were released from the LSM surface and diffused to the electrolyte surface where the nuclei were formed [7].

Similar studies were conducted by Jiang et al. wherein the LSM electrode was replaced by a platinum electrode [8]. For the case of a platinum cathode, Jiang et al. claimed that degradation of cell performance occurs but deposition of chromium species was not observed on the electrolyte or the platinum surface. This observation suggested that the reduction of chromium vapor from the environment was not the main source of the cell degradation [8].

Jiang et al. also performed an experiment where an LSM electrode was replaced by LSCF [8]. Chromium contamination was observed with both the absence and presence of current through the cathode of the fuel cell. The contamination often takes place on the surface of the LSCF, forming strontium chromium oxide columnar structure $SrCrO_4$ and Cr_2O_3 [8]. Quadakkers et al. applied a layer of lanthanum strontium cobalt oxide $(La,Sr)CoO_3$ on a chromium oxide-forming alloy [9]. The specimen was heated at 900 °C for 1000 h. Strontium from the specimen completely reacted with the chromium oxide alloy, forming a Sr depleted layer on the specimen [9]. Acid etching of the LSCF electrode before operation could enhance the performance of the fuel cell, due to the removal of Sr ions from LSCF [9]. Jiang et al. noted less deposition of strontium chromium species when 200 mA current was applied to the LSCF electrode [8]. This suggested segregation of Sr ions from the surface of LSCF in the presence of current could improve the fuel cell performance [9]. Both observation from Jiang and Quadakkers suggested that the rate of reaction between LSCF and chromium oxide is affected by both chemistry and electrochemistry in nature [8,9].

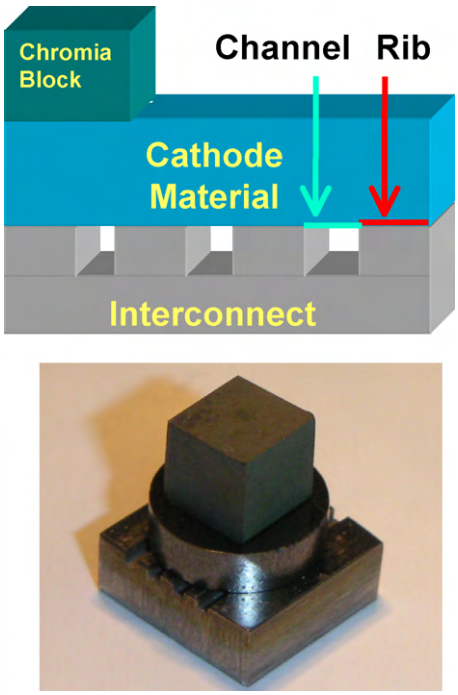

Fig. 1. Layout of the specimen stack where the cathode material pellet is placed between a chromium block and stainless steel interconnect coupon.

LNF cathodes were investigated by Komatsu et al. and found to have high tolerance to chromium deposition when compared to LSM [11]. Chromium deposited and reacted with LSM forming various chromium compounds at the cathode/electrolyte interface, whereas chromium distributed homogenously on the LNF structure, without reacting [11].

1.2. Solid state diffusion mechanism

The bulk of the Cr–cathode interaction literature focuses on vapor transport of Cr species. Tucker et al. found solid state diffusion to be another pathway of chromium contamination [12]. They investigated the reaction of individual oxides and metals with Cr via both solid state diffusion and vapor deposition mechanisms at 700–1000 °C [12]. Ferritic stainless steel powder was placed on top of the oxide samples in a chromium-saturated atmosphere for 150 h. There was a clear difference between the vapor deposition and solid state diffusion mechanisms on the extent of chromium contamination of the single oxide and metal materials. Other literature, however, only reported on the vapor deposition mechanism [2–5] without considering the solid state diffusion mechanism.

The present study also considers the migration of Cr species through solid state diffusion when no electrochemistry is involved. It is important to understand the relative Cr transport and reaction rates in order to evaluate the most viable commercially available cathode material.

2. Experimental methods

A mixture of 10 g $La_{0.65}Sr_{0.3}MnO_3$ (LSM, Praxair Inc.), 0.2 g of menhaden fish oil (MFO), 0.2 g of poly(vinyl butyral–co vinyl alcohol–co–vinyl acetate) (PVB) and 0.2 g of dibutyl phthalate (DBT) is ball milled for 24 h in isopropyl alcohol (IPA). The mixture is dried, grinded and sieved to <150 μm. The powder is then pressed into 1 cm diameter pellets under the uniaxial hydrostatic press at

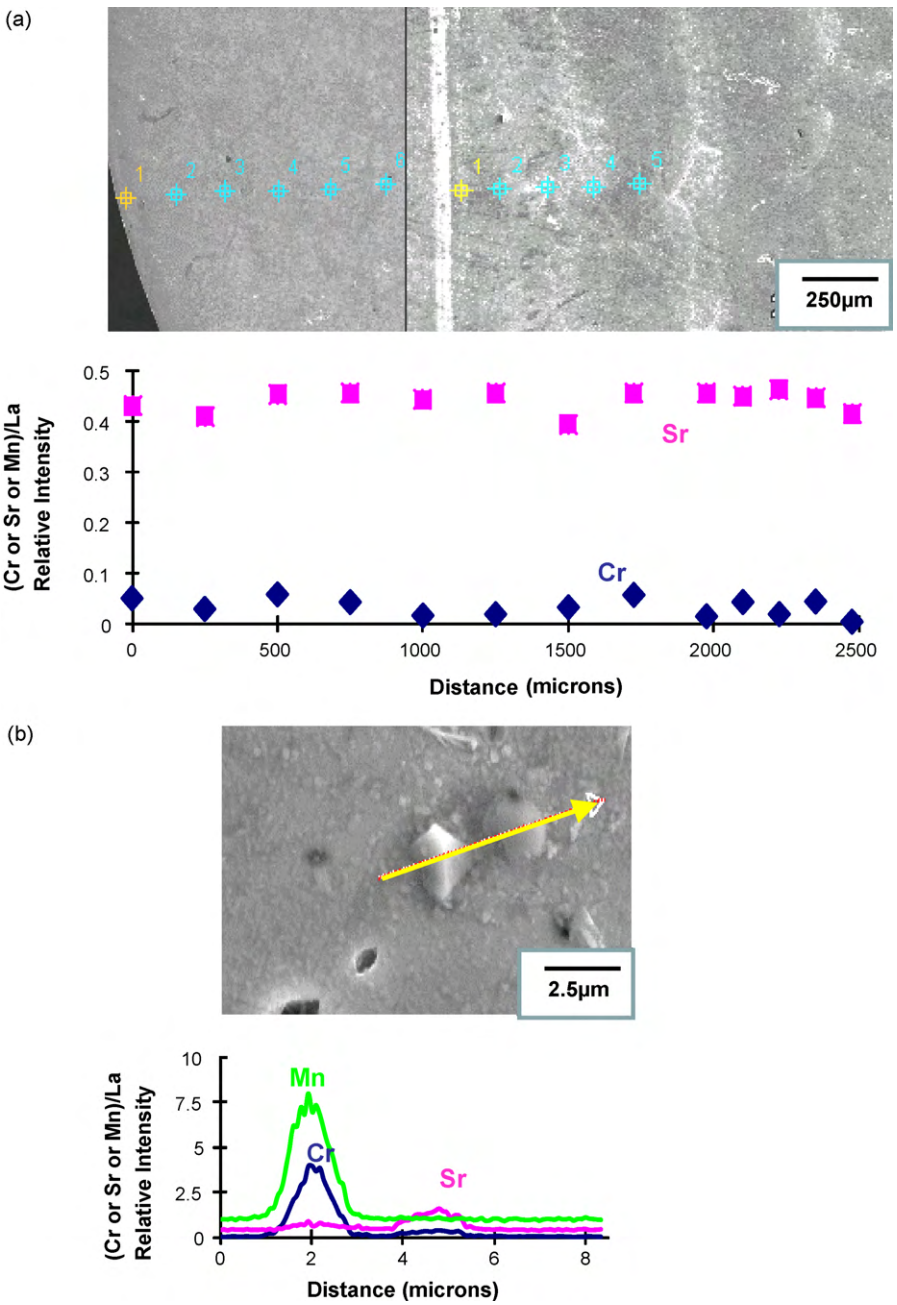

Fig. 2. (a) SEM image and EDS point scans of strontium and chromium content of LSM pellet on Cr block after the experiment. (b) SEM image and EDS line scans of strontium, chromium and magnesium content across LSM pellet on chromium block after the experiment.

~70 MPa for 30 s. The above procedure is repeated for the two other cathode materials $La_{0.6}Sr_{0.4}Fe_{0.8}Co_{0.2}O_3$ (LSCF, Praxair Inc.) and $La_{0.98}Ni_{0.6}Fe_{0.4}O_3$ (LNF, Praxair Inc.).

The cathode pellets are sintered at 900 °C (LSCF), 1200 °C (LSM) and 1200 °C (LNF) for 10 h. The 95–98% dense cathode pellets, along with (99%) pure chromium blocks (Alfa Aesar Inc.) and 410 stainless steel interconnects are polished to ~1 μm. The chromium blocks are pre-oxidized at 950 °C for 2 h to provide an abundant source of chromium oxide for reaction. Fig. 1 shows the layout of the specimen stack where the pellet is placed between a chromium block and a stainless steel interconnect coupon.

The specimen stacks are exposed to chromium-saturated atmosphere at 700 °C for 300 h. The atmosphere is saturated with water by inserting a stream of inlet flowing gas (filtered house air), with water [12]. The glassware setup for the experiment is explained by Kurokawa et al. [13]. The partial pressure of Cr species is controlled by the oxygen partial pressure and the water vapor saturator. The chromium-saturated atmosphere is done by placing high-surface-area pieces of chromium oxide blocks on the upstream of the specimen.

At 700 °C operation, the pO_2 is set to 0.2 atm, and pH_2O is set to 0.083 atm [12]. By using the thermodynamic values calculated by Ebbinghaus, the $\log(PCrO_2(OH)_2)$ is −6.34 atm [14]. The specimen stacks are reacted at 700 °C for 300 h. Then a detailed analysis of the transport of chromium is done by using XRD (Siemens D500, X-ray Diffraction), SEM (Hitachi S4300SE/N, Scanning Electron Microscope), EDS (Hitachi S4300SE/N, Energy Dispersive Spectroscopy) and FIB (Focused Ion and Electron Beam; FEI Strata 235M).

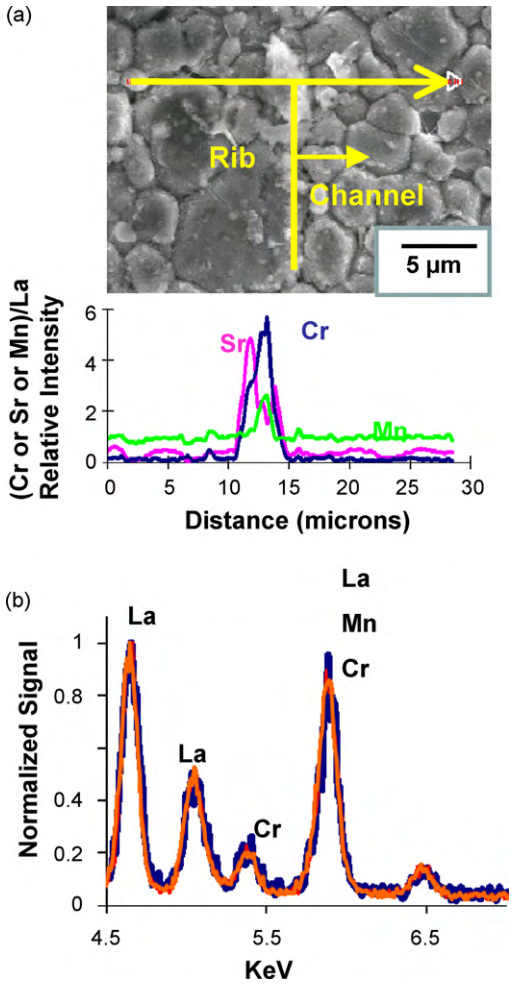

Fig. 3. (a) SEM image and EDS line scans of LSM surface at the edge of the interconnect rib. (b) EDS elemental analysis of LSM pellet at the rib and channel before and after the experiment.

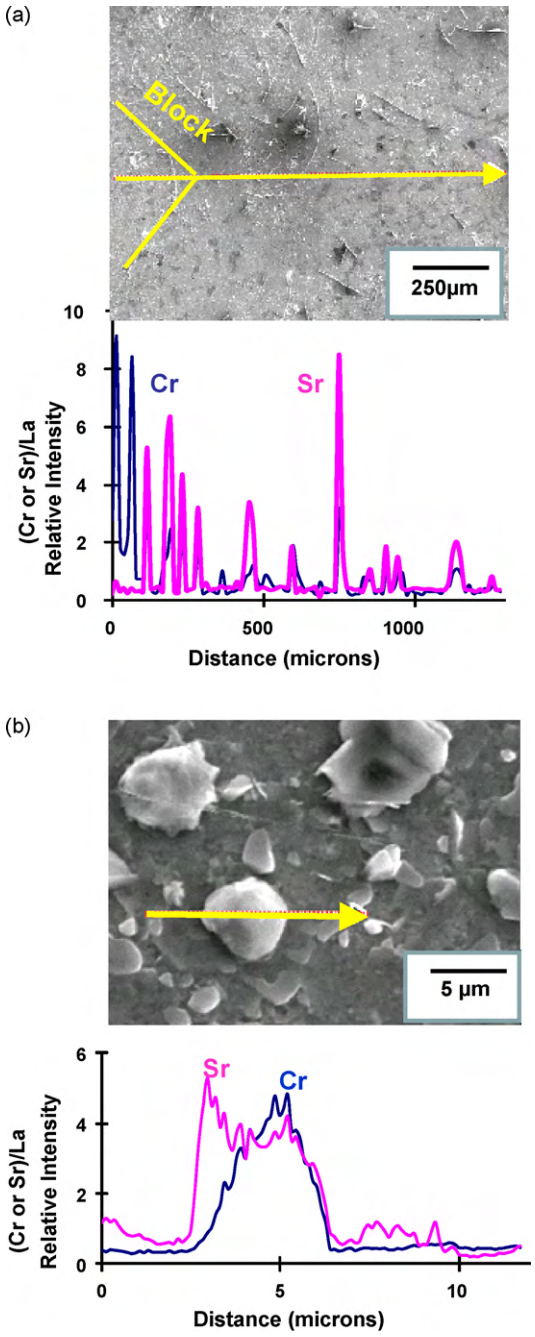

Fig. 4. (a) SEM image and EDS line scans of the strontium and chromium content across the LSCF pellet beneath the corner of the chromium block to the end of the LSCF pellet after the experiment. (b) SEM image and EDS line scans of strontium and chromium content across LSCF pellet directly under the surface of the chromium block.

3. Results

3.1. Lanthanum strontium manganese oxide interaction with chromium block and stainless steel interconnect

LSM along with a piece of chromium block and a piece of stainless steel interconnect were exposed to Cr-saturated atmosphere at 700 °C for 300 h. Several EDS line scans were performed across the surface of the LSM pellet near the corner of the Cr block. Peak intensities for Cr, Sr and Mn are normalized to La (most abundant source in LSM), providing a relative concentration. Fig. 2a is taken from the edge of the LSM pellet towards the middle of the LSM pellet where the Cr block was in contact. The point scan in Fig. 2a shows a uniform concentration of Sr and minimal Cr on the surface of the LSM pellet. This suggests that negligible amount of Cr is adsorbed/deposited on the surface of the LSM pellet by chemical reaction. Cr compounds are not detected on the LSM surface away from the Cr block, suggesting vapor deposition of Cr from the Cr-saturated atmosphere did not occur on LSM. The line scan in Fig. 2b shows a higher magnification of the LSM surface at the contact area between the Cr block and the LSM pellet. Small amounts of localized Sr–Cr and Mn–Cr compounds are detected, suggesting reaction of Cr with LSM during the experiment.

Additional EDS line scans were performed across the portion of the LSM pellet that had been in contact with the stainless steel interconnect during the experiment. Fig. 3a shows small amounts of Sr–Cr and Mn–Cr compounds segregated along the edge of the interconnect rib. This initiates noticeable LSM interaction with the edge of the stainless steel interconnect occurs during annealing. Fig. 3b compares the elemental scans for the LSM pellet before reaction, LSM pellet contacting the rib, and the LSM pellet above the channel of the stainless steel interconnect. The relative intensity is fairly consistent for the three scans, suggesting minimal reaction between the LSM and the stainless steel interconnect during the experiment. These observations are consistent with the work of Taniguchi et al. which showed little reactivity between LSM and Cr when the fuel cell was held at open circuit potential [4]. Vigorous

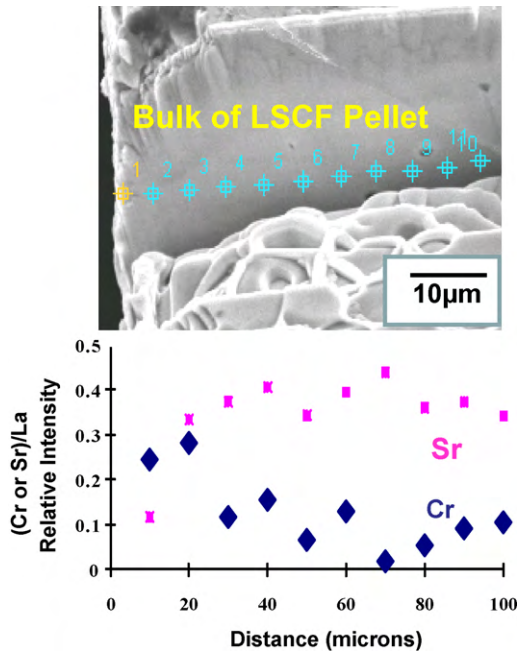

Fig. 5. Study of chromium diffusion of the LSCF pellet using Focused Ion Beam (FIB).

reaction, leading to the depletion of Sr, is expected when LSM is undergoing an electrochemical reaction [4].

3.2. Lanthanum strontium cobalt ferrite interaction with the chromium block and the stainless steel interconnect

LSCF specimen stack was being analyzed after 300 h of operation and EDS X-ray line scans were performed across the surface of the LSCF pellet near the corner of the Cr block as shown in Fig. 4a. Peak intensities for Cr and Sr were normalized to La, providing relative concentrations. A large amount of Cr is adsorbed/deposited nonuniformly on the surface of the LSCF pellet. In the area away from the block, LSCF was in contact with Cr-saturated air. Cr is deposited nonuniformly from the vapor phase. A more uniform, higher concentration of Cr is observed underneath the block, suggesting solid state diffusion of Cr from the block to the LSCF surface. In both areas, high concentrations of Sr are observed in conjunction with the Cr deposition. This shows the Cr reacted with LSCF, extracting Sr to form a Sr–Cr rich compound along the surface of the LSCF pellet [8,10]. Fig. 4b shows a higher magnification of the surface of the LSCF pellet around the surface of the Cr block. Large amounts of Sr–Cr compounds are observed on the LSCF surface directly under the surface and far away from the Cr block. These observations are consistent with the results of previous work that indicates LSCF will form reaction products with Cr at high temperatures without the presence of current [8,10]. Since the surface of the LSCF pellet reacted vigorously with Cr, analysis in the bulk of the LSCF pellet beneath the Cr block was also performed.

A bulk analysis was performed by removing a small part of the LSCF pellet using milling Focused Ion Beam (FIB). Depletion of Sr and adsorption of Cr is evident at the surface of the LSCF pellet, as shown in Fig. 5, indicates adsorption/solid state diffusion occurred beneath the Cr block. Quantitative approximations of Cr diffusion and Sr depletion are not appropriate in this instance as only surface reaction (first 10–20 μm) is observed on the LSCF pellet. The concentration of Sr and Cr is relatively uniform, and no observable trend for Sr or Cr diffusion is observed in the bulk of the LSCF pellet, as shown in Fig. 5.

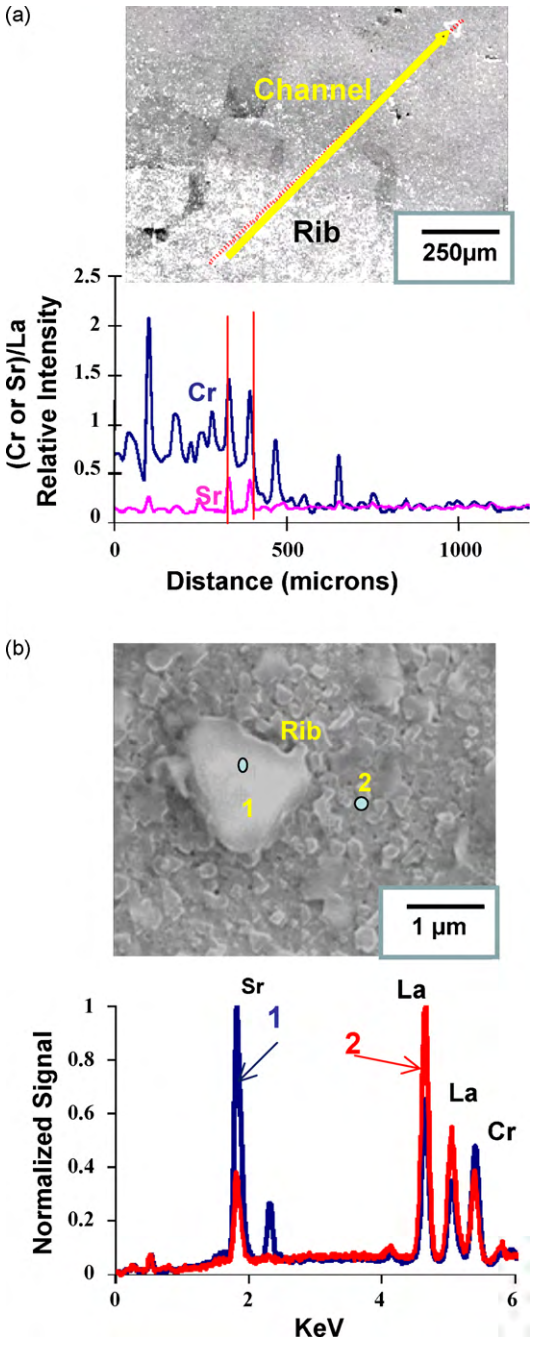

Fig. 6. (a) SEM image and EDS line scans on the strontium and chromium content of the LSCF pellet on the stainless steel interconnect channel/rib boundary. (b) SEM image and EDS elemental analysis on the rib of the LSCF pellet.

EDS X-ray line scans were also performed along the surface of the LSCF pellet on top of the stainless steel interconnect after the experiment. The line scan data in Fig. 6a, indicates Cr from the stainless steel interconnect is adsorbed/deposited on the surface of the LSCF pellet. The two red lines on the lower graph in Fig. 6a highlight areas of substantial reaction between Sr from the LSCF pellet and Cr from the stainless steel interconnect. Fig. 6b shows a higher magnification image of the "rib area" of the LSCF pellet. The spectrum obtained from the reaction product (point 1) shows a clear Sr-enrichment in contrast with the spectrum recoded at the LSCF surface (point 2) which is consistent with the stoichiometric LSCF.

LSCF reacted vigorously with the Cr block and the stainless steel interconnect, therefore, more analysis was done to check the sur-

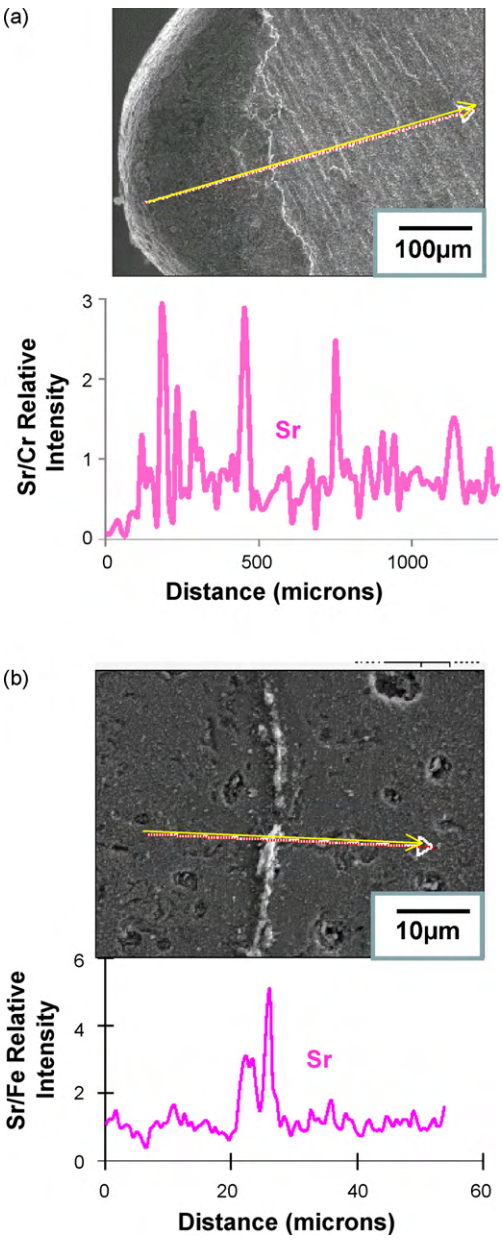

Fig. 7. (a) SEM image and EDS line scans on the content of strontium at the surface of the chromium block after the experiment. (b) SEM image and EDS line scans on the content of strontium at the surface of the stainless steel interconnect after the experiment.

face of the Cr block along with the stainless steel interconnect after the experiment. Fig. 7a and b indicates that Sr from LSCF migrates to the surface of the Cr block and the edges of the LSCF pellet on the stainless steel interconnect. The above observations are consistent with the literature where Jiang and Quadakkers suggested the reaction between LSCF and chromium oxide occurs chemically in nature [8–10].

3.3. Lanthanum nickel ferrite interaction with chromium block and stainless steel interconnect

LNF reacted differently with the Cr block and the stainless steel interconnect as compared to LSM and LSCF. Cr deposits are seen everywhere from the edge of the Cr block on the LNF surface to the stainless steel interconnect side of the LNF pellet. Significant amount of Cr deposits are observed on the surface of the LNF surface where the edge of the Cr block was originally located as shown in Fig. 8a and b. The relative intensity of Ni and Fe decreased while the Cr intensity increased in the line scan, Cr enrichment on the LNF pellet makes the detection of Ni–Cr or Fe–Cr compounds difficult. While Cr is adsorbed/deposited on the LNF surface, minimal reaction occurs.

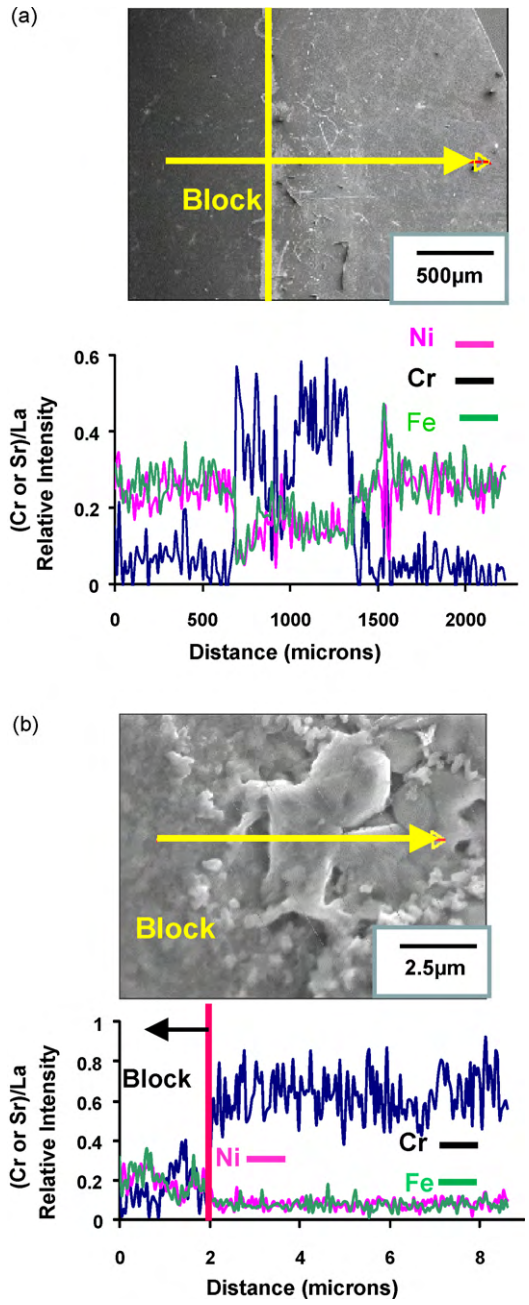

Fig. 8. (a) SEM image and EDS line scans on the content of chromium, nickel and ferrite of the LNF pellet after reacting with chromium block for after the experiment. (b) SEM image and EDS line scans on the content of chromium, nickel and ferrite of the LNF pellet at the Cr deposition layer along the edge of the Cr block.

The mechanical bond between the stainless steel and LNF pellet is stronger than that of the Cr block and LNF pellet. A cutting blade was used to separate the LNF pellet from the stainless steel interconnect. Presumably, the mechanical bond is due to Cr compounds that deposited on the LNF surface as seen in the EDX scans shown in Fig. 9a. Fig. 9b magnified the boundary between the rib and the channel. The larger grain along the channel side essentially forms a “blanket of Cr” on top of the LNF pellet along the channel area.

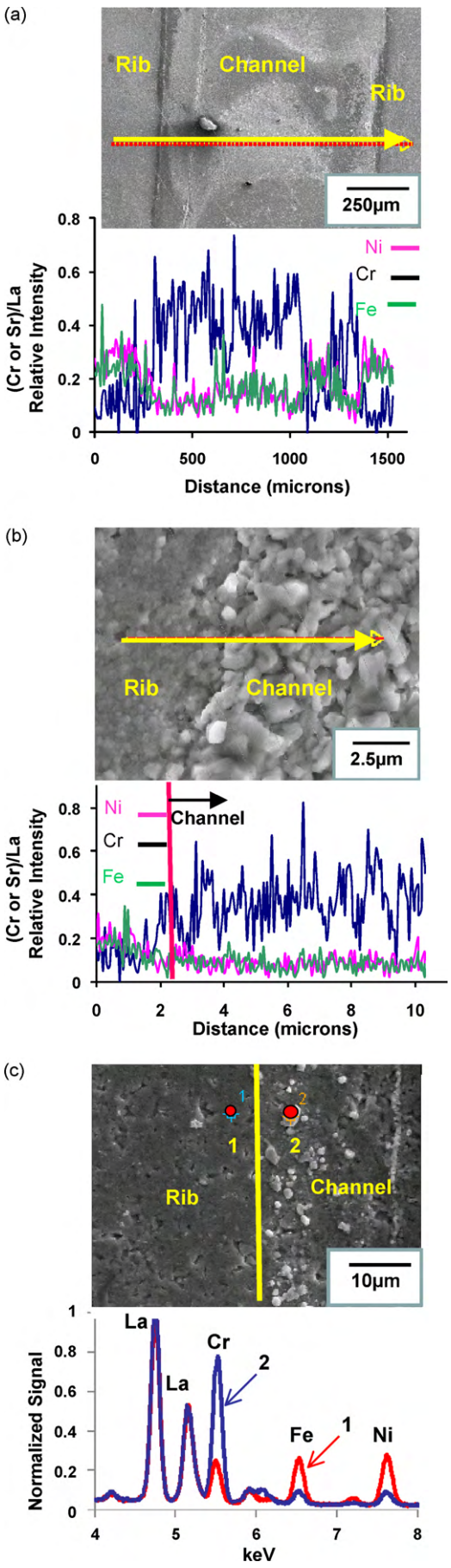

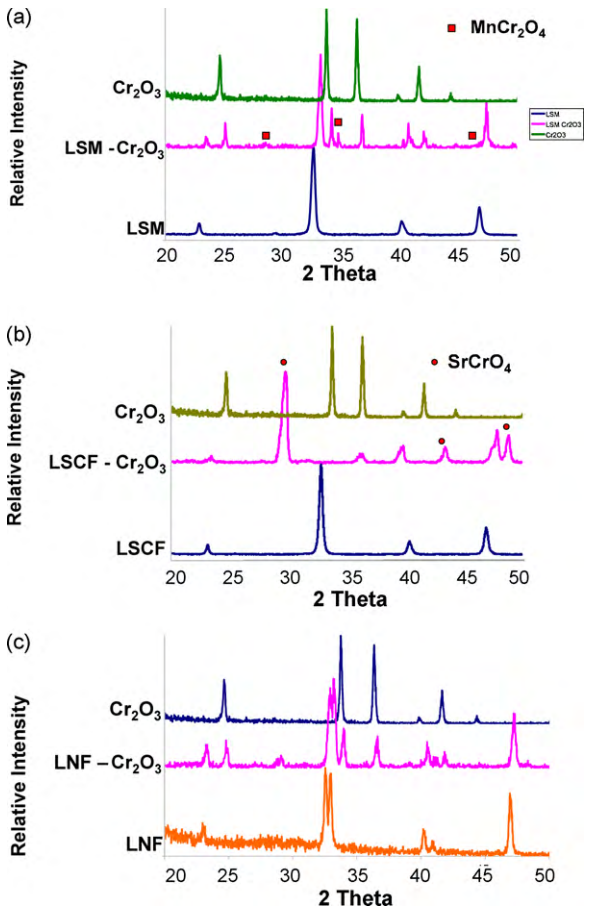

Fig. 10. (a) XRD pattern of LSM and chromium oxide (Cr_2O_3) reaction couple. (b) XRD pattern of LSCF and chromium oxide (Cr_2O_3) reaction couple. (c) XRD pattern of LNF and chromium oxide (Cr_2O_3) reaction couple.

The Cr on the channel area of the LNF pellet makes it difficult to detect if there is reaction between Ni–Cr or Fe–Cr along the surface as indicated on the EDS elemental analysis between the rib and the channel of the LNF pellet in Fig. 9c. However, no Cr deposit is observed on the rib area where the stainless steel interconnect was in direct contact with the LNF pellet. Detection of Cr deposits is difficult on the rib area as the LNF pellet was stuck onto the stainless steel interconnect rib during the experiment and was being lifted off when separating the stainless steel interconnect from the LNF pellet.

3.4. Reaction couples

For a cathode material to be Cr-tolerant, it must be chemically stable in contact with Cr-containing materials. To assess chemical compatibility, LSM, LSCF and LNF are mixed with Cr_2O_3 and pressed to pellets. The pellets were held at 700 °C for 300 h in air. X-ray diffraction (XRD) was used to determine the extent of reaction. Fig. 10 compares XRD patterns for the mixtures to those of pure chromia and cathode materials. For the case of LSM, several peaks of $MnCr_2O_4$ are identified as shown in Fig. 10a, which indicates reaction between LSM and the Cr_2O_3 compounds. Note,

Fig. 9. (a) SEM image and EDS line scans on the content of chromium, nickel and ferrite of the LNF pellet at the stainless steel interconnect. (b) SEM image and EDS line scans on the content of chromium, nickel and ferrite from the rib to the channel part of the LNF pellet. (c) SEM image and EDS elemental analysis at the rib and the channel of the LNF pellet after the experiment.

however, that the pattern is dominated by peaks associated with pure Cr_2O_3 and LSM, suggesting only reaction. As for LSCF (Fig. 10b), strong peaks of $SrCrO_4$ oxide are observed and no pure Cr_2O_3 or LSCF is retained, indicating vigorous reaction between LSCF and Cr_2O_3. Minimal reaction is detected in the case of LNF (Fig. 10c); where most of the LNF and Cr_2O_3 phases are retained and there are minimal additional peaks for the mixture.

4. Discussion

Chromium (Cr) transport on various cathode materials was investigated after heating in air at 700 °C for 300 h. Cr transport on LSM is observed along the edges of the chromium block and the ribs of the stainless steel interconnect suggesting possible solid state surface diffusion occurred at those areas. Small amounts of Mn–Cr and Sr–Cr compounds are formed, indicating minor reactivity between LSM and Cr. The Sr content in LSM remains fairly uniform throughout the whole LSM pellet. These observations are consistent with the literature of Taniguchi et al. wherein they observed little reactivity between LSM and Cr when the fuel cell was held at open circuit potential [4]. Vigorous reaction, leading to the depletion of Sr, is expected when LSM is undergoing an electrochemical reaction [4].

Cr transport on LSCF is observed to occur via both solid state surface diffusion and vapor deposition. The reaction between Cr and LSCF is the most severe among the three cathode materials studied. Sr is presumably extracted from the LSCF, forming various Sr–Cr compounds with the chromium block and the stainless steel interconnect. These compounds tend to form along the edges of the chromium block and the ribs of the stainless steel interconnect.

Cr transport on LNF is also observed along the edges of the chromium block and channels of the stainless steel interconnect, suggesting solid state surface diffusion occurred during the experiment. However, no chromium–LNF reaction products are observed on the surface of the LNF pellet indicating LNF did not react with Cr. This is in contrast to the results for LSM and LSCF, and may be due to the absence of Sr, Co or Mn which are known to be chromium nucleation sites for the cathode materials [15]. Therefore, LNF is proposed to be the most chromium tolerant cathode material in this experiment.

It is important to understand the relative Cr transport and reaction rates to evaluate the most viable commercially available cathode material. This study characterizes the migration of Cr species through solid state diffusion and vapor deposition. Similar reactions and products have been found between the chromia block and the stainless steel interconnect coupon. Based on the above observations, it is proposed that both geometry and reaction couple experiment should be conducted to ensure different aspects of the Cr transport are investigated for each cathode material.

5. Conclusion

Chromium blocks and stainless steel interconnects were placed in contact with cathode materials at 700 °C (the optimum intermediate SOFC operating temperature) for 300 h. Cr transport by solid state surface diffusion is observed on LSM, LSCF and LNF. Cr transport by vapor deposition is not observed on LSM but is significant on both LSCF and LNF. LSCF reacts severely with Cr, LSM shows minor reaction, and no detectable reaction with Cr is observed for LNF.

In general, a new type of experiment has been designed to help clarify the different modes of Cr transport pathways such as vapor deposition, solid state diffusion, effects of surface energy, and chemical reaction. XRD analysis on Cr–cathode reaction couples is an easy experiment to screen out different Cr-tolerant cathode materials. Mixtures of Cr powder and cathode materials decreased the diffusion distance to sub-microns providing the worst Cr-contamination environment for observation.

Acknowledgements

I would like to thank Dr. Hideto Kurokawa for help in this project. This project was sponsored in part by NETL through the SECA program by the US Department of Energy under the contract number DE-AC03-76SF00098.

References

[1] H. Kurokawa, K. Kawamura, T. Maruyama, Solid State Ionics 168 (2004) 13–21.
[2] Z. Yang, Int. Mater. Rev. 53 (2008) 39–54.
[3] N. Minh, T. Takahashi, Science and Technology of Ceramic Fuel Cells, Elsevier Science, Amsterdam, Netherlands, 1995, pp. 1–13.
[4] S. Taniguchi, M. Kadowaki, H. Kawamura, T. Yasuo, Y. Akiyama, Y. Miyake, T. Saitoh, J. Power Sources 55 (1995) 77–79.
[5] K. Hilpert, D. Das, M. Miller, D. Peck, R. Weiss, J. Electrochem. Soc. 143 (1996) 3642–3647.
[6] S.P. Jiang, J.P. Zhang, K. Foger, J. Electrochem. Soc. 147 (2002) 3195–3205.
[7] S.P. Jiang, J.P. Zhang, K. Foger, J. Electrochem. Soc. 148 (2001), pp. 477–455.
[8] S.P. Jiang, J.P. Zhang, X.G. Zheng, J. Eur. Ceram. Soc. 22 (2002) 361–373.
[9] W.J. Quadakkers, H. Greiner, M. Hansel, A. Pattanaik, A.S. Khanna, W. Mallener, Solid State Ionics 91 (1996) 55–67.
[10] S.P. Jiang, Solid State Ionics 146 (2002) 1–22.
[11] T. Komatsu, H. Arai, R. Chiba, K. Nozawa, M. Arakawa, K. Sato, J. Electrochem. Soc. 154 (2007) B379–B382.
[12] M.C. Tucker, H. Kurokawa, C.P. Jacobson, L.C. De Jonghe, S.J. Visco, J. Power Sources 106 (2006) 130–138.
[13] H. Kurokawa, C.P. Jacobson, L.C. DeJonghe, S.J. Visco, Solid State Ionics 178 (2007) 287–296.
[14] B.B. Ebbinghaus, Combust. Flame 93 (1993) 119–137.
[15] R. Chiba, F. Yoshimura, Y. Sakurai, Solid State Ionics 124 (1999) 281–288.